Robotica (2021), **39**, pp. 1518–1535
doi:10.1017/S0263574720001319

CAMBRIDGE UNIVERSITY PRESS

RESEARCH ARTICLE

Active fault-tolerant control of a Schoñflies parallel manipulator based on time delay estimation

Pegah Ghaf-Ghanbari, Mahmood Mazare and Mostafa Taghizadeh*

Faculty of Mechanical and Energy Engineering, Shahid Beheshti University, Tehran, Iran
E-mails: pegah.g.ghanbari@gmail.com, m_mazare@sbu.ac.ir
*Corresponding author. Email: mo_taghizadeh@sbu.ac.ir

Received: 9 April 2020; **Revised:** 12 November 2020; **Accepted:** 8 December 2020; **First published online:** 19 April 2021

Keywords: Fault-tolerant control (FTC); Terminal sliding mode; Time delay estimation (TDE); Parallel robot; Schönflies motion generator

Abstract

In this paper, a new hybrid fault-tolerant control (FTC) strategy based on nonsingular fast integral-type terminal sliding mode (NFITSM) and time delay estimation (TDE) is proposed for a Schönflies parallel manipulator. In order to detect, isolate, and accommodate actuator faults, TDE is used as an online fault estimation algorithm. Stability analysis of the closed-loop system is performed using Lyapunov theory. The proposed controller performance is compared with conventional sliding mode and feedback linearization control methods. The obtained results reveal the superiority of the proposed FTC based on TDE and NFITSM.

1. Introduction

During the past few decades, robotic systems have found their way into different technological sectors, especially for high-risk, repetitive, and high-precision tasks. The complex and challenging environment in which these robotic systems are employed makes them highly sensitive to components failure, either those happen to sensors, actuators, or the system. In general, conventional control systems cannot compensate for the detrimental effects of faults and may end up with loss of performance, instability, or even complete failure. Grave concern for the risks associated with faults, especially those affecting safety, reliability, and performance, has made the fault-tolerant control (FTC) an indispensable part of the robotic system design process which can enhance system reliability and ensure the effectiveness of the control system in the presence of unexpected faults [1]. Successful implementation of this approach to various applications has proven its effectiveness in diverse fields such as spacecrafts [2, 3], robotics, [4, 5, 6, 7] and energy [8, 9, 10]. In general, FTC can be categorized into two types, passive FTC (PFTC) and active FTC (AFTC). In PFTC, a robust control scheme is designed for both normal and faulty operations. To be able to deal with any unpredicted fault, the controller needs to be highly robust. On the other hand, PFTC does not rely on fault detection (FD) information, so it is fast in compensating for the effects of faults [11]. In contrast, AFTC relies on FD, isolation, and accommodation and mostly shows superior performance over the passive approach. Once the fault is detected, the controller is reconfigured to adjust the control input and compensate for the effects of fault [12].

Different approaches have been proposed for FD, including intelligent learning techniques [12, 13, 14] sliding mode observer (SMO) [15, 16, 17], or a combination of these approaches [4, 18]. However, intelligent techniques suffer from high computational cost and difficult implementation, and the SMO method requires the pre-knowledge about bounds of faults which in most practical cases is not known. Combining these approaches alleviates their problems to some extent, but their difficult implementation still persists. Time delay estimation (TDE) is a simple, model-free, yet robust approach

which can be effectively applied for FD [19]. For FTC purpose of robotic manipulators, different strategies have been adopted, mainly based on computed torque control (CTC) [18, 20], backstepping [11], neural networks,12 model predictive,7 and sliding mode control (SMC) [4, 5].

SMC scheme is robust against uncertainties and external disturbances, and less sensitive to the system parameter variations. However, it suffers from chattering and infinite-time convergence to equilibrium point, which can cause serious problem during system operation. These problems are addressed by some modifications on the conventional method. For finite-time convergence of the states to the equilibrium point, terminal SMC (TSMC) has been proposed.21 However, there exist two major concerns. First, its convergence rate is lower than conventional SMC when the system state is far away from the equilibrium point. Second, it has singularity problem. As a solution to the first problem, fast terminal sliding mode (FTSM) control is devised, [22] and the second problem is addressed through nonsingular TSMC (NTSMC)23 and the nonsingular fast TSMC (NFTSMC) [24].

In robotic literatures, various approaches have been adopted to promote the performance of SMC-based FTC [25]. Meng et al. [4] designed ASMFTC for an uncertain Stewart platform which does not require fault diagnosis process. By offline computing or parallel computing based on nominal multibody dynamics, the initial upper bound is calculated and a novel adaptive updating law is employed to reduce the conservativeness and alleviate the chattering. Van et al.11 proposed an adaptive backstepping NFTSMC which has the robustness, fast transient response, and finite-time convergence of NFTSMC, as well as globally asymptotic stability of backstepping control strategy. The dependency of the controller on pre-knowledge of the bounds of faults is eliminated by applying an adaptive method. These researchers also developed a robust controller by integrating a self-tuning fuzzy proportional integral derivative (PID) control-NFTSMC and a TDE.26 Their proposed controller offers fast transient response with finite-time convergence, low steady-state error, and chattering elimination. The PID gains are tuned using a fuzzy logic system and the unknown dynamic model is estimated via a TDE algorithm.

In this paper, a new hybrid FTC strategy is proposed for a Schönflies parallel manipulator with pick-and-place application in the presence of actuator faults and external disturbances. The key contributions of this paper are summarized as follows:

(1) A new AFTC is proposed by combining adaptive nonsingular fast integral-type terminal sliding mode (ANFITSM) and TDE, which can compensate the model uncertainties, especially those associated with complicated dynamic modeling of the parallel manipulators.
(2) ANFITSM ensures high robustness against uncertainties and disturbances, improves transient response, and offers fast convergence to the desired states.
(3) By employing adaptive law, the need for excessive high gain is eliminated, which results in lower control effort and reduced chattering.
(4) For FD, TDE algorithm is applied, which is a model-free approach and eliminates the requisite bounds of faults and uncertainties.

The rest of the paper is organized as follows. In Section 2, the parallel manipulator is introduced. Sections 3 and 4 deal with kinematic and dynamic analysis. Trajectory planning is presented in Section 5. Section 6 is devoted to fault diagnosis based on TDE algorithm, and FTC based on ANFITSM. Simulation results are discussed in Section 7, and the paper is concluded in Section 8.

2. Manipulator description

The mechanism under review is a modification on redundantly actuated Veloce manipulator, [27] comprising of four identical R-$(SS)^2$ arms, connecting a base to an end-effector. By shifting the connection of the two opposite arms to the end-effector along opposite directions of the base frame, and adding two revolute joints as shown in Fig. 1, the mechanism will be able to generate Schönflies motion, with its rotation around horizontal axis [28].

https://doi.org/10.1017/S0263574720001319 Published online by Cambridge University Press

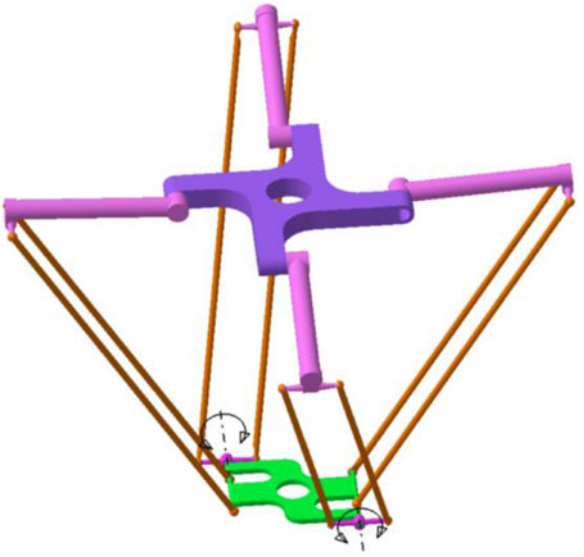

Figure 1. *CAD model of Schönflies motion robot.*

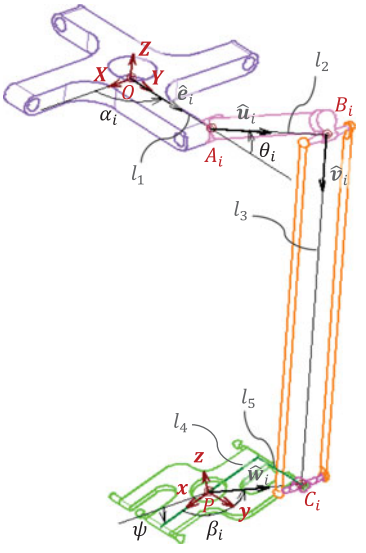

Figure 2. *Coordinate frames and variables of the arm.*

3. Kinematics

The structure of one arm of the manipulator is illustrated in Fig. 2. The base frame $\mathfrak{F}_O{:}O-XYZ$ is attached to the geometric center of the fixed platform, defined by revolute joints $(A_i,\ i=1,\ldots,\ 4)$, with its X direction pointing towards A_1 and its Z direction normal to the plane of the fixed platform. Similarly, the moving frame $\mathfrak{F}_P{:}P-xyz$ is set at the geometric center of the moving platform, with its x direction crossing point C_1 and its z direction perpendicular to the plane formed by C_i , $(i=1,\ \ldots,\ 4)$, representing the attaching points of the arms to the end-effector. y is the rotation axis of the end-effector and it always remains parallel to Y.

https://doi.org/10.1017/S0263574720001319 Published online by Cambridge University Press

The loop-closure equation for the ith arm is written as

$$\mathbf{r}_P + \varepsilon_i l_4 \widehat{\boldsymbol{w}}_i = \mathbf{r}_{Ai} + l_2 \widehat{\boldsymbol{u}}_i + l_3 \widehat{\boldsymbol{v}}_i \tag{1}$$

$$\varepsilon_i = \begin{cases} \sec \beta_i & i = 1,\ 4 \\ -\sec \beta_i & i = 2,\ 3 \end{cases} \tag{2}$$

Rearranging this equation and squaring both sides yields the constraint equations of the manipulator as,

$$\boldsymbol{f}\ (\mathcal{X}, \boldsymbol{\Theta}) = (\mathbf{r}_P + \varepsilon_i l_4 \widehat{\boldsymbol{w}}_i - \mathbf{r}_{Ai})^2 + l_2^2 - 2l_2\ (\mathbf{r}_P + \varepsilon_i l_4 \widehat{\boldsymbol{w}}_i - \mathbf{r}_{Ai})\ .\widehat{\boldsymbol{u}}_i - l_3^2 = \mathbf{0} \tag{3}$$

where $\mathcal{X} = \left[\ \mathbf{r}_P^T\ \psi\ \right]^T$ is the end-effector pose, and $\boldsymbol{\Theta} = \left[\ \theta_1\ \theta_2\ \theta_3\ \theta_4\ \right]^T$ is the active joint variables.

For velocity analysis, Jacobian matrix is extracted by differentiating Eq. (1) with respect to time.

$$\dot{\mathbf{r}}_P = l_2\ (\boldsymbol{\omega}_{Ui} \times \widehat{\boldsymbol{u}}_i) + l_3\ (\boldsymbol{\omega}_{Li} \times \widehat{\boldsymbol{v}}_i) - \varepsilon_i l_4 \left(\dot{\boldsymbol{\psi}} \times \widehat{\boldsymbol{w}}_i\right) \tag{4}$$

where $\boldsymbol{\omega}_{Ui}$ and $\boldsymbol{\omega}_{Li}$ are the angular velocity of the upper and lower links of the ith arm, respectively. Taking the dot product of both sides of Eq. (4) with $\widehat{\boldsymbol{v}}_i$ and considering $\boldsymbol{\omega}_{Ui} = \dot{\theta}_i \widehat{\boldsymbol{n}}_i$, we obtain

$$\dot{\mathbf{r}}_P . \widehat{\boldsymbol{v}}_i = l_2 \dot{\theta}_i\ (\widehat{\boldsymbol{n}}_i \times \widehat{\boldsymbol{u}}_i)\ .\widehat{\boldsymbol{v}}_i - \varepsilon_i l_4 \dot{\psi}\ \left(\hat{j} \times \widehat{\boldsymbol{w}}_i\right) .\widehat{\boldsymbol{v}}_i \tag{5}$$

This gives a mapping between the velocity of the ith active joint and the end-effector, which can be written in the following matrix form:

$$\begin{aligned} &\boldsymbol{J}_X \dot{\mathcal{X}} = \boldsymbol{J}_\theta \dot{\boldsymbol{\Theta}}, \\ &\boldsymbol{J}_{Xi} = \left[\ \widehat{\boldsymbol{v}}_i^T\ \ \varepsilon_i l_4 \left(\hat{j} \times \widehat{\boldsymbol{w}}_i\right) .\widehat{\boldsymbol{v}}_i\ \right], \quad \boldsymbol{J}_X = \left[\ \boldsymbol{J}_{X1}^T\ \boldsymbol{J}_{X2}^T\ \boldsymbol{J}_{X3}^T\ \boldsymbol{J}_{X4}^T\ \right]^T, \\ &J_{\theta i} = l_2\ (\widehat{\boldsymbol{n}}_i \times \widehat{\boldsymbol{u}}_i)\ .\widehat{\boldsymbol{v}}_i, \qquad \boldsymbol{J}_\theta = \mathrm{diag}\left[\ J_{\theta 1}\ J_{\theta 2}\ J_{\theta 3}\ J_{\theta 4}\ \right]. \end{aligned} \tag{6}$$

Obviously, the velocity equation for the whole manipulator will be

$$\dot{\mathcal{X}} = \boldsymbol{J} \dot{\boldsymbol{\Theta}}, \boldsymbol{J} = \boldsymbol{J}_X^{-1} \boldsymbol{J}_\theta\ . \tag{7}$$

where $\dot{\boldsymbol{\Theta}} = \left[\ \dot{\theta}_1\ \dot{\theta}_2\ \dot{\theta}_3\ \dot{\theta}_4\ \right]^T$ represents the vector of active joints angular velocity and $\dot{\mathcal{X}} = \left[\ \dot{\mathbf{r}}_P^T\ \dot{\psi}\ \right]^T$ is the velocity of the end-effector.

4. Dynamics

For dynamic modeling of the manipulator, Euler–Lagrange formulation for constrained systems is used. As the rotational inertia of the lower links is negligible, they are considered as point masses on their both extreme ends [29].

For modeling a dynamic system using Euler–Lagrange formulation, the first step is determining the Lagrangian, which is defined by

$$\mathcal{L}\left(\boldsymbol{\Theta}, \dot{\boldsymbol{\Theta}}, \mathcal{X}, \dot{\mathcal{X}}\right) = T\left(\boldsymbol{\Theta}, \dot{\boldsymbol{\Theta}}, \mathcal{X}, \dot{\mathcal{X}}\right) - U(\boldsymbol{\Theta}, \mathcal{X}) \tag{8}$$

Here, the only conservative force stored in the form of potential energy is gravity.

$$\begin{aligned} &U(\boldsymbol{\Theta}, \mathcal{X}) = U_a(\boldsymbol{\Theta}) + U_p(\mathcal{X})\ , \\ &U_a(\boldsymbol{\Theta}) = -\frac{1}{2}\ (m_U + m_L)\ \mathrm{g} l_2 \sum_{i=1}^{4} \sin \theta_i\ . \\ &U_p(\mathcal{X}) = -m_e \mathrm{g} z_p. \end{aligned} \tag{9}$$

https://doi.org/10.1017/S0263574720001319 Published online by Cambridge University Press

Table I. *Parameters of the manipulator.*

Parameter	Value (m)	Parameter	Value
l_1	0.2	m_u	0.4 kg
l_2	0.3	m_L	0.2 kg
l_3	0.8	m_p	0.1 kg
l_4	0.11	I_{pyy}	1.56×10^{-3}kg·m^2
l_5	0.11	–	–

with subscripts a and p representing arm and moving platform, respectively. Kinetic energy of the manipulator is obtained from

$$\begin{aligned} T\left(\dot{\boldsymbol{\Theta}}, \dot{\mathcal{X}}\right) &= T_a\left(\dot{\boldsymbol{\Theta}}\right) + T_p\left(\dot{\mathcal{X}}\right), \\ T_a\left(\dot{\boldsymbol{\Theta}}\right) &= \frac{1}{12} l_2^2 \left(2m_U + 3m_L\right) \dot{\boldsymbol{\Theta}}^T \dot{\boldsymbol{\Theta}}, \\ T_p\left(\dot{\mathcal{X}}\right) &= \frac{1}{2} \dot{\mathcal{X}}^T \boldsymbol{M}_e \dot{\mathcal{X}}. \end{aligned} \tag{10}$$

where $\boldsymbol{M}_e = \text{diag}\left[\, m_e \boldsymbol{I}_{3\times 3} \; I_{e_{yy}} \,\right], m_e = m_p + 2m_L, \quad I_{e_{yy}} = I_{p_{yy}} + 2m_L l_4^2$. It is obvious that the Lagrangian can be written as the contribution of two subsystems, each one depending on its own variables, though connected together via constraint equations. The dynamic model of the arms is written as

$$\boldsymbol{I}_a \ddot{\boldsymbol{\Theta}} + \boldsymbol{G}_a = \boldsymbol{\tau} + \left(\frac{\partial \boldsymbol{f}}{\partial \boldsymbol{\Theta}}\right)^T \boldsymbol{\lambda} \tag{11}$$

$$\boldsymbol{I}_a = \left(\frac{1}{3} m_U + \frac{1}{2} m_L\right) l_2^2 \boldsymbol{I}_{4\times 4} \tag{12}$$

$$\boldsymbol{G}_a = -\frac{1}{2} l_2 \left(m_U + m_L\right) \text{gcos}\, \boldsymbol{\Theta} \tag{13}$$

where $\boldsymbol{\lambda}_{4\times 1}$ is the vector of Lagrange multipliers. Similarly, the dynamic model of the end-effector is calculated as

$$\boldsymbol{M}_e \ddot{\mathcal{X}} + \boldsymbol{G}_p = \boldsymbol{F}_{E,p} + \left(\frac{\partial \boldsymbol{f}}{\partial \mathcal{X}}\right)^T \boldsymbol{\lambda} \tag{14}$$

$$\boldsymbol{G}_p = \begin{bmatrix} 0 & 0 & -m_e \text{g} & 0 \end{bmatrix}^T \tag{15}$$

where $\boldsymbol{F}_{E,p}$ is the external wrenches applied to the end-effector. In order to calculate the dynamic model of the whole manipulator, these two models are combined by cancelling the Lagrange multipliers as follows:

$$\begin{aligned} \boldsymbol{\tau} &= \mathcal{M}\ddot{\boldsymbol{\Theta}} + \mathcal{C}\dot{\boldsymbol{\Theta}} + \mathcal{G} + \mathcal{F} \\ \mathcal{M} &= \boldsymbol{I}_a + \boldsymbol{J}^T \boldsymbol{M}_e \boldsymbol{J}, \qquad \mathcal{C} = \boldsymbol{J}^T \boldsymbol{M}_e \dot{\boldsymbol{J}} \\ \mathcal{G} &= -\left(\boldsymbol{G}_a + \boldsymbol{J}^T \boldsymbol{G}_p\right), \qquad \mathcal{F} = -\boldsymbol{J}^T \boldsymbol{F}_{E,p}. \end{aligned} \tag{16}$$

Parameters of the manipulator are listed in Table I.

5. Trajectory planning

In spite of the fact that capability and efficiency of parallel robots are directly related to their dynamic characteristics and controller, a proper trajectory planning also plays a crucial role in smooth torques, low energy consumption, low residual vibrations, and short cycle times.

https://doi.org/10.1017/S0263574720001319 Published online by Cambridge University Press

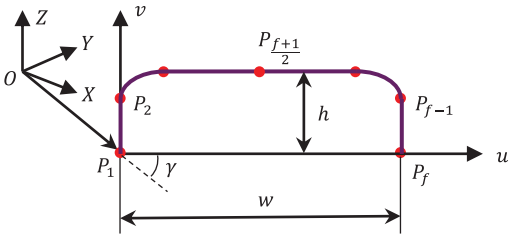

Figure 3. *Geometric path defined in a local frame.*

Based on the approach presented by Li et al. [30] an optimal smooth pick-and-place trajectory is designed using fifth order B-spline curves which guarantee C^4-continuity and ensures jerk-free departure and arrival. To this end, a geometric path comprising of $f = 5$ via points is generated in a local frame as shown in Fig. 3. Any point on the path can be defined in the base frame by coordinate transformation.

A B-spline of degree q and order $k = q + 1$ is a linear combination of polynomials $N_{i,q}(t)$ of degree q, called *base* or *blending functions*, weighted by control points, Q_i. t represents a normalized independent parameter here taken as the time. Then, the normalized motion profile, $s(t)$, is formed as

$$s(t) = \sum_{i=1}^{n} Q_i . N_{i,q}(t) \,, \quad 0 \le t \le 1 \tag{17}$$

The base function is defined recursively by means of the De Boor formula [31].

$$\begin{cases} N_{i,0}(t) = \begin{cases} 1, \; t_i \le t < t_{i+1} \\ 0, \; \text{elsewhere} \end{cases} \\ N_{i,q}(t) = \frac{t - t_i}{t_{i+q} - t_i} N_{i,q-1}(t) + \frac{t_{i+q+1} - t}{t_{i+q+1} - t_{i+1}} N_{i+1,q-1}(t) \end{cases} \tag{18}$$

t_i ($i = 1, 2, \ldots, m = n + q + 1$) is a sequence of nodes on which $s(\tau)$ is built by interpolation. In order for the control points to coincide with the initial and final via points, the nodes at both ends of the trajectory must be repeated $q + 1$ times. Moreover, to obtain trajectories with no jerk at both ends, two virtual points are introduced at the second and second-last position of the node sequence. With these considerations, the number of nodes and the number of control points will be $m = 2(q + 1) + f$ and $n = q + f + 1$, respectively. Therefore, the sequence of nodes is written as

$$\left\{ \underbrace{0, \; 0, \; \ldots, \; 0}_{6}, \, t_7, \underbrace{t_8, \, t_9, \, t_{10}}_{3}, \, t_{11}, \underbrace{1, \; 1, \; \ldots, \; 1}_{6} \right\} \tag{19}$$

Accordingly, two time ratios are defined as

$$k_1 = t_8 / t_9, \qquad k_2 = t_7 / t_8 \tag{20}$$

where $0 < k_1 < 1$ is the ratio between the time that the end-effector spends to move from P_1 to P_2 and the time from P_1 to P_3. $0 < k_2 < 1$ represents the ratio between the time that the end-effector spends to move from P_1 to P_{v1} and the time from P_1 to P_2.

The rth derivative of B-spline is calculated from:

$$\frac{d^r s}{dt^r} = \sum_{i=1}^{n-r} Q_{i,r} . N_{i,q-r}(t) \tag{21}$$

where $Q_{i,r}$ represents the control points of the rth derivative of $s(t)$ and can be deduced recursively by

$$Q_{i,r} = \begin{cases} Q_i, & r = 0 \\ \frac{q - r + 1}{\tau_{i+q+1} - \tau_{i+r}} \left(Q_{i+1,r-1} - Q_{i,r-1} \right), & 0 < r \le q \end{cases} \tag{22}$$

https://doi.org/10.1017/S0263574720001319 Published online by Cambridge University Press

Imposing boundary conditions for position, velocity, acceleration, and jerk, control points are calculated which are used to build trajectories along u and v axes. Position vector of any point on the path can be deduced from:

$$\mathbf{r}(t) = \left[u(t)\ v(t) \right]^T = \left[w\ s_u(t)\ h\ s_v(t) \right]^T, \quad t = t/T \tag{23}$$

where subscripts "u" and "v" stand for motion profile along the horizontal and vertical axis in local frame.

As the peak values and smoothness of the time histories of the active joint torques are directly related to those of acceleration and jerk of the end-effector at nonsingular configurations, we can optimize the trajectory in the Cartesian space using appropriate performance indices based on acceleration and jerk of the end-effector[32]. To ensure that the trajectory has minimum acceleration and jerk, their maximum amounts are chosen as indices for the optimization problem in which k_1 and k_2 are taken as variables.

$$\begin{aligned} a_{\max}(k_1, k_2) &= \max_{0 \le \tau \le 1} \|\boldsymbol{a}(\tau)\| \\ j_{\max}(k_1, k_2) &= \max_{0 \le \tau \le 1} \|\boldsymbol{j}(\tau)\| \end{aligned} \tag{24}$$

The multi-objective optimization problem for the smooth trajectory is formulated as:

$$\begin{aligned} &\text{Minimize } f_1(\mathbf{x}) = a_{\max} \\ &\text{Minimize } f_2(\mathbf{x}) = j_{\max} \\ &\text{Over } \mathbf{x} = [k_1\ k_2] \\ &\text{Subject to } \begin{matrix} g_1\colon 0 < k_1 < 1 \\ g_2\colon\ 0 < k_2 < 1 \end{matrix} \end{aligned} \tag{25}$$

6. AFTC based on TDE and ANFITSMC

Actuator fault is a serious problem in robotics, since it has the potential to damage both the robot components and their environment. Evidently, for robotic applications implementing FTC is of high importance. FD is an indispensable part of AFTC which in most common approaches requires the bounds of faults. In this work, TDE algorithm, a simple and model-free approach, is applied as a robust FD scheme to detect, isolate, and estimate the unknown uncertainties and faults. The proposed ANFITSM offers high accuracy and robustness, fast convergence rate, and eliminated chattering. The terminal term guarantees finite-time convergence of the tracking error to zero from any initial value, and the integral term eliminates the reaching phase, ensuring the robustness from the initial state. The singularity problem of conventional TSMC is eliminated, and the reliance on the prior knowledge of the upper bound of the uncertainties is removed by introducing an adaptive mechanism.

6.1. FTC based on ANFITSM

The dynamic model of the four-degrees of freedom parallel robot in the presence of uncertainties and actuator fault is written as [25]

$$\mathcal{M}\ddot{\boldsymbol{\Theta}} + \mathcal{C}\dot{\boldsymbol{\Theta}} + \mathcal{G} + \mathcal{F} + \boldsymbol{\Phi} + \boldsymbol{\sigma} = \boldsymbol{\tau} \tag{26}$$

where $\boldsymbol{\sigma}$ denotes uncertainties and $\boldsymbol{\Phi} = \boldsymbol{\nu}\left(t - T_f\right)\phi$ represents actuator fault**,** in which ϕ is the fault vector and $\boldsymbol{\nu}\left(t - T_f\right)$ is its time profile, defined by:

$$\nu_i\left(t - T_f\right) = \begin{cases} 0 & t < T_f \\ 1 - e^{-\delta_i}\left(t - T_f\right) & t \ge T_f \end{cases} \tag{27}$$

in which δ_i is the evolution rate of the unknown fault.

https://doi.org/10.1017/S0263574720001319 Published online by Cambridge University Press

In order to use time delay control, a positive diagonal gain matrix, $\widetilde{\boldsymbol{M}}$, is introduced to the dynamic equation, which results in

$$\begin{aligned}\widetilde{\boldsymbol{M}}\ddot{\boldsymbol{\Theta}}+\boldsymbol{H}\left(\boldsymbol{\Theta},\dot{\boldsymbol{\Theta}},\ddot{\boldsymbol{\Theta}}\right)&=\boldsymbol{\tau},\\ \boldsymbol{H}\left(\boldsymbol{\Theta},\dot{\boldsymbol{\Theta}},\ddot{\boldsymbol{\Theta}}\right)&=\left[\mathcal{M}\left(\boldsymbol{\Theta},\dot{\boldsymbol{\Theta}}\right)-\widetilde{\boldsymbol{M}}\right]\ddot{\boldsymbol{\Theta}}+\mathcal{C}\left(\boldsymbol{\Theta},\dot{\boldsymbol{\Theta}}\right)\dot{\boldsymbol{\Theta}}+\mathcal{G}\left(\boldsymbol{\Theta}\right)+\mathcal{F}\left(\boldsymbol{\Theta},\dot{\boldsymbol{\Theta}}\right)\\ &\quad+\boldsymbol{\nu}\left(t-T_f\right)\phi\left(\boldsymbol{\Theta},\dot{\boldsymbol{\Theta}},\boldsymbol{\tau}\right)+\boldsymbol{\sigma}.\end{aligned}\tag{28}$$

Here, the time variable, t, is not shown for simplicity reason, except for the time profile. Now, the sliding manifold and its time derivative for ANFITSM control scheme are defined as follows:

$$\boldsymbol{S}=\dot{\boldsymbol{e}}+2\mu\boldsymbol{e}+\mu^2\int\boldsymbol{e}dt+c_1\boldsymbol{e}^{r_1/r_2}+c_2\boldsymbol{e}^{\varphi}\tag{29}$$

$$\dot{\boldsymbol{S}}=\ddot{\boldsymbol{e}}+2\mu\dot{\boldsymbol{e}}+\mu^2\boldsymbol{e}+\frac{r_1}{r_2}c_1\boldsymbol{e}^{\frac{r_1-r_2}{r_2}}\dot{\boldsymbol{e}}+c_2\varphi\boldsymbol{e}^{\varphi-1}\dot{\boldsymbol{e}}=\boldsymbol{0}\tag{30}$$

where $\boldsymbol{e}=\boldsymbol{\Theta}-\boldsymbol{\Theta}_d$ is the error vector, and μ, c, and c_2 are positive gains. For the controller to have nonsingular property, $\varphi>r_1/r_2$, and r_1 and r_2 are chosen odd integers satisfying $1<r_1/r_2<2$.

Expanding $\ddot{\boldsymbol{e}}$ and substituting Eq. (28) into Eq. (30), the following equation holds:

$$\widetilde{\boldsymbol{M}}^{-1}\left(\boldsymbol{\tau}-\boldsymbol{H}\right)-\ddot{\boldsymbol{\Theta}}_d+2\mu\dot{\boldsymbol{e}}+\mu^2\boldsymbol{e}+\frac{r_1}{r_2}c_1\boldsymbol{e}^{\frac{r_1-r_2}{r_2}}\dot{\boldsymbol{e}}+c_2\varphi\,\boldsymbol{e}^{\varphi-1}\dot{\boldsymbol{e}}=\boldsymbol{0}\tag{31}$$

The chosen sliding manifold eliminates the reaching phase and provides an ideal sliding motion ($\dot{\boldsymbol{S}}=\boldsymbol{S}=\boldsymbol{0}$). Thus, the matched uncertainties are compensated during the entire system response and the unmatched ones are improved as reported in ref. [33].

The ANFITSM-FTC control law in the presence of actuator faults is chosen as

$$\boldsymbol{\tau}=\widehat{\boldsymbol{H}}+\widetilde{\boldsymbol{M}}\left[\ddot{\boldsymbol{\Theta}}_d+2\mu\dot{\boldsymbol{e}}+\mu^2\boldsymbol{e}+\frac{r_1}{r_2}c_1\boldsymbol{e}^{\frac{r_1-r_2}{r_2}}\dot{\boldsymbol{e}}+c_2\varphi\boldsymbol{e}^{\varphi-1}\dot{\boldsymbol{e}}+\boldsymbol{\rho}\boldsymbol{S}\right]\tag{32}$$

in which $\widehat{\boldsymbol{H}}$ is the estimation of $\boldsymbol{H}$, and the gain matrix, $\boldsymbol{\rho}$, satisfies the following gain dynamics:[34]

$$\dot{\rho}_{ii}=\gamma_{ii}\left|S_i\right|\operatorname{sgn}\left(\left|S_i\right|-\frac{\rho_{ii}^2}{\phi_i}\right)\tag{33}$$

where $\boldsymbol{\gamma}$and ϕ represent the adaptation gain matrix and the normalizing factor for tracking accuracy adjustment.

Based on TDE, when the sampling delay, L, is sufficiently small, $\widehat{\boldsymbol{H}}$ can be approximated by $\boldsymbol{H}_{t-L}$ [35, 36]. In practice, the sampling delay, L, is chosen as the sampling time to ensure that L is sufficiently small. So, Eq. (28) is written as

$$\boldsymbol{H}\left(\boldsymbol{\Theta},\dot{\boldsymbol{\Theta}},\ddot{\boldsymbol{\Theta}}\right)\approx\widehat{\boldsymbol{H}}\left(\boldsymbol{\Theta},\dot{\boldsymbol{\Theta}},\ddot{\boldsymbol{\Theta}}\right)=\boldsymbol{H}_{t-L}\left(\boldsymbol{\Theta},\dot{\boldsymbol{\Theta}},\ddot{\boldsymbol{\Theta}}\right)=\boldsymbol{\tau}_{t-L}-\widetilde{\boldsymbol{M}}\ddot{\boldsymbol{\Theta}}_{t-L}\tag{34}$$

It is noteworthy that the plant does not comprise any time delay. By introducing the time delay to the dynamic equation, the nonlinear and uncertain terms of the robot dynamics are estimated and cancelled [33, 35, 36]. The ANFITSM with TDE and gain dynamics is proposed as

$$\boldsymbol{\tau}=\boldsymbol{\tau}_{t-L}-\widetilde{\boldsymbol{M}}\ddot{\boldsymbol{\Theta}}_{t-L}+\widetilde{\boldsymbol{M}}\left[\ddot{\boldsymbol{\Theta}}_d+2\mu\dot{\boldsymbol{e}}+\mu^2\boldsymbol{e}+\frac{r_1}{r_2}c_1\,\boldsymbol{e}^{\frac{r_1-r_2}{r_2}}\dot{\boldsymbol{e}}+c_2\varphi\boldsymbol{e}^{\varphi-1}\dot{\boldsymbol{e}}+\boldsymbol{\rho}\boldsymbol{S}\right]\tag{35}$$

In the gain dynamics, Eq. (33), following conditions hold:

(i) if $|S_i|>\rho_{ii}^2/\vartheta_i$:

The gain matrix increases, leading to reduced TDE error as well as tracking error.

(ii) if $|S_i|<\rho_{ii}^2/\vartheta_i$:

The gain matrix decreases, preventing an excessive high gain when the control error is acceptable.

https://doi.org/10.1017/S0263574720001319 Published online by Cambridge University Press

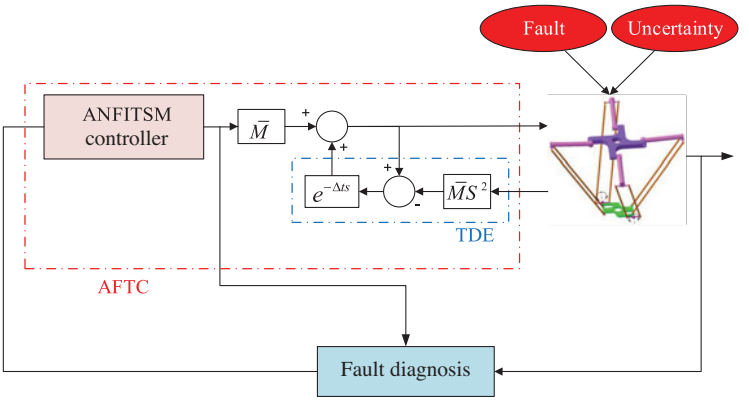

Figure 4. *Block diagram of the proposed AFTC.*

The term ρ_{ii}^2/ϑ_i determines tracking accuracy of the controller and can be regarded as an acceptance layer. Smaller values for the acceptance layer show better tracking accuracy. The normalizing factor, ϑ_i, tunes the size of $\rho_{ii}^2$with respect to $|S_i|$, and thus guarantees tracking accuracy with proper magnitude of control inputs.

Depending on the choice of gain matrix, different previously proposed formulations are derived. For constant gain matrix, the proposed controller becomes Jin's formulation [33, 37], and for zero gain matrix, it becomes Hsia's formulation [35, 36]. The constant gain matrix is manually tuned by trial-and-error and is signified as $\boldsymbol{\rho} = \varrho \boldsymbol{I}$ (where ϱ is a positive constant) [33, 37].

Parameter variation is an intrinsic characteristic of the robot manipulators, since their posture is continually changing during operation. Thus, the gains are posture related, and it is not possible to find an optimal gain for the entire operation range[38] The adaptive nature of the proposed controller gives the opportunity to handle these parameter variations, through adaptive auto-tuning of $\boldsymbol{\rho}$ with Eq. (33).

Fig. 4 illustrates the proposed controller. The sliding manifold employed in this controller eliminates the reaching phase, prevents the singularity problem, and enhances the robustness. The adaptive gain $\boldsymbol{\rho}$ is tuned as a proper positive value to ensure acceptable tracking accuracy. The nonzero positive value of this gain can offer instantaneous control action to eliminate the TDE error caused by abrupt disturbances and faults.

The closed-loop system with the proposed control scheme is uniformly, ultimately bounded.

Lemma 1. *If the control gain, $\widetilde{\boldsymbol{M}}$, is chosen to satisfy the following inequality:*

$$\left\| \boldsymbol{I} - \mathcal{M}^{-1}(\boldsymbol{\Theta}) \widetilde{\boldsymbol{M}} \right\| < 1, \qquad \forall t \geq 0$$

then, $\left\| \ddot{\boldsymbol{\Theta}}_{t-L} - \ddot{\boldsymbol{\Theta}}_t \right\| \to 0$ as $L \to 0$ and the TDE errors are bounded, that is, $\left\| H_i - \hat{H}_i \right\|_\infty \leq \varepsilon_i^+$.

Lemma 2. *The variable control gain, ρ_{ii}, is bounded by $\rho_{ii}^+ = \sqrt{\|\boldsymbol{S}\|_\infty \vartheta_i}$ for $t \geq 0$. The closed-loop dynamics can be defined as*

$$\frac{S_i}{\varepsilon_i} = \frac{1}{\tilde{M}_{ii}} \frac{1}{(d/dt) + \rho_{ii}} \tag{36}$$

Thus, if TDE error, ε_i, is bounded, S_i is bounded by a first-order low-pass filter.

As mentioned earlier, adaptation law can create two ranges, $|S_i| > \rho_{ii}^2/\vartheta_i$ and $|S_i| < \rho_{ii}^2/\vartheta_i$.

For the first range, the inequality can be rewritten as $\rho_{ii} < \sqrt{|S_i|\,\vartheta_i}$, in which ρ_{ii} increases with $\dot{\rho}_{ii} = \gamma_{ii}\,|S_i|$. Based on Eq. (33), when $|S_i|$ is maximum, $\rho_{ii}$is bounded by $\rho_{ii}^+ = \sqrt{\|\boldsymbol{S}\|_\infty \vartheta_i}$ for $t \geq 0$.

Theorem. *Considering the adaptive control law Eq. (33), the parallel robot system with the proposed TDE-ANFITSM control law is stable and its states tend to their desired values, if the following condition is satisfied:*

https://doi.org/10.1017/S0263574720001319 Published online by Cambridge University Press

$$\vartheta_i \|\boldsymbol{S}\|_\infty < \frac{\left|\varepsilon_i^+ - \varepsilon_i\right|^2}{\tilde{M}_{ii}^2} \tag{37}$$

Proof. A positive definite Lyapunov function is chosen as:

$$V = \frac{1}{2}\boldsymbol{S}^T\boldsymbol{S} + \frac{1}{2}\sum_{i=1}^{n}\frac{1}{\gamma_{ii}}\left(\rho_{ii} - \tilde{M}_{ii}^{-1}\varepsilon_i^+\right)^2 \tag{38}$$

and its time derivative is written as:

$$\begin{aligned}
\dot{V} &= \boldsymbol{S}^T\dot{\boldsymbol{S}} + \frac{1}{\gamma_{ii}}\left(\rho_{ii} - \tilde{M}_{ii}^{-1}\varepsilon_i^+\right)\dot{\rho}_{ii} \\
&= \boldsymbol{S}^T\left(\tilde{\boldsymbol{M}}^{-1}\boldsymbol{\varepsilon} - \boldsymbol{\rho}\boldsymbol{S}\right) + \sum_{i=1}^{n}\left(\rho_{ii} - \tilde{M}_{ii}^{-1}\varepsilon_i^+\right)|S_i| \\
&\le \sum_{i=1}^{n}\left[-\rho_{ii}S_i^2 + \tilde{M}_{ii}^{-1}\varepsilon_i\,|S_i| + \left(\rho_{ii} - \tilde{M}_{ii}^{-1}\varepsilon_i^+\right)|S_i|\right] \\
&\le -\sum_{i=1}^{n}\rho_{ii}S_i^2 + \sum_{i=1}^{n}\left[\left(\rho_{ii} - \tilde{M}_{ii}^{-1}\left|\varepsilon_i^+ - \varepsilon_i\right|\right)|S_i|\right]
\end{aligned} \tag{39}$$

If $\rho_{ii} < \tilde{M}_{ii}^{-1}\left|\varepsilon_i^+ - \varepsilon_i\right|$, it is concluded that $\dot{V} < 0$. In other words, the sliding variable, $\boldsymbol{S}$, varies in the range defined by $|S_i| < \rho_{ii}^2/\vartheta_i$. Due to the fact that $\dot{V}$ is indefinite in this range, the sliding variable $\boldsymbol{S}$ may repeatedly cross the acceptance layer ρ_{ii}^2/ϑ_i.

When $\boldsymbol{S}$ is in the range $|S_i| > \rho_{ii}^2/\vartheta_i$, the time derivative of Lyapunov function becomes negative definite ($\dot{V} < 0$).

If ϑ_i is chosen to satisfy the condition defined by Eq. (37), it is inferred that the inequality $\rho_{ii} \le \rho_{ii}^+ < \tilde{M}_{ii}^{-1}\left|\varepsilon_i^+ - \varepsilon_i\right|$ holds. According to the Lemma 2, ρ_{ii} is bounded as $\rho_{ii} \le \rho_{ii}^+ = \sqrt{\|\boldsymbol{S}\|_\infty \vartheta_i}$ in the range $\forall\,|S_i| > \rho_{ii}^2/\vartheta_i$. Provided that $\sqrt{\|\boldsymbol{S}\|_\infty \vartheta_i} < \tilde{M}_{ii}^{-1}\left|\varepsilon_i^+ - \varepsilon_i\right|$, it can be concluded that ρ_{ii} is always less than $\tilde{M}_{ii}^{-1}\left|\varepsilon_i^+ - \varepsilon_i\right|$, and the condition is set as $\vartheta_i\|\boldsymbol{S}\|_\infty < \left|\varepsilon_i^+ - \varepsilon_i\right|^2/\tilde{M}_{ii}^2$. As a result, the closed-loop system with ρ_{ii} is stable. □

6.2. *Fault diagnosis using TDE*

For sufficiently small time delay value (L), the uncertainty ($\boldsymbol{\sigma}$) and fault ($\boldsymbol{\Phi}$) can be estimated by a continuous or piecewise continuous function as

$$\begin{aligned}
\boldsymbol{\sigma}(\boldsymbol{\Theta}, \dot{\boldsymbol{\Theta}}, \boldsymbol{\tau})_t &\cong \boldsymbol{\sigma}(\boldsymbol{\Theta}, \dot{\boldsymbol{\Theta}}, \boldsymbol{\tau})_{t-L} \\
\boldsymbol{\Phi}(\boldsymbol{\Theta}, \dot{\boldsymbol{\Theta}}, \boldsymbol{\tau})_t &\cong \boldsymbol{\Phi}(\boldsymbol{\Theta}, \dot{\boldsymbol{\Theta}}, \boldsymbol{\tau})_{t-L}
\end{aligned} \tag{40}$$

Based on the above assumption, the approximation of $\boldsymbol{\sigma}$ and $\boldsymbol{\Phi}$ is determined as follows:

$$\begin{aligned}
\widehat{\boldsymbol{\sigma}}(\boldsymbol{\Theta}, \dot{\boldsymbol{\Theta}}, \boldsymbol{\tau})_t &\triangleq \boldsymbol{\sigma}\left(\boldsymbol{\Theta}, \dot{\boldsymbol{\Theta}}, \boldsymbol{\tau}\right)_{t-L} \\
\widehat{\boldsymbol{\Phi}}(\boldsymbol{\Theta}, \dot{\boldsymbol{\Theta}}, \boldsymbol{\tau})_t &\triangleq \boldsymbol{\Phi}\left(\boldsymbol{\Theta}, \dot{\boldsymbol{\Theta}}, \boldsymbol{\tau}\right)_{t-L}
\end{aligned} \tag{41}$$

Then, by merging Eqs. (40) and (41)Error! Reference source not found., the TDE can be shown as

$$\begin{aligned}
&\widehat{\boldsymbol{\sigma}}(\boldsymbol{\Theta}, \dot{\boldsymbol{\Theta}}, \boldsymbol{\tau})_t + \widehat{\boldsymbol{\Phi}}(\boldsymbol{\Theta}, \dot{\boldsymbol{\Theta}}, \boldsymbol{\tau})_t \triangleq \boldsymbol{\sigma}\left(\boldsymbol{\Theta}, \dot{\boldsymbol{\Theta}}, \boldsymbol{\tau}\right)_{t-L} + \boldsymbol{\Phi}\left(\boldsymbol{\Theta}, \dot{\boldsymbol{\Theta}}, \boldsymbol{\tau}\right)_{t-L} \\
&= \left(\mathcal{M}\ddot{\boldsymbol{\Theta}} + \mathcal{C}\dot{\boldsymbol{\Theta}} + \mathcal{G} - \boldsymbol{\tau}\right)_{t-L} \\
&= \mathfrak{R}_{TDE}
\end{aligned} \tag{42}$$

https://doi.org/10.1017/S0263574720001319 Published online by Cambridge University Press

Table II. *Trajectory and controller parameters.*

Parameter	Value	Parameter	Value
k_1	0.31	M	$0.003\mathbf{I}_{4x4}$
k_1	0.12	r_1	9
μ	10	r_2	7
c_1	7	φ	1.5
C_2	6	ϑ	800000

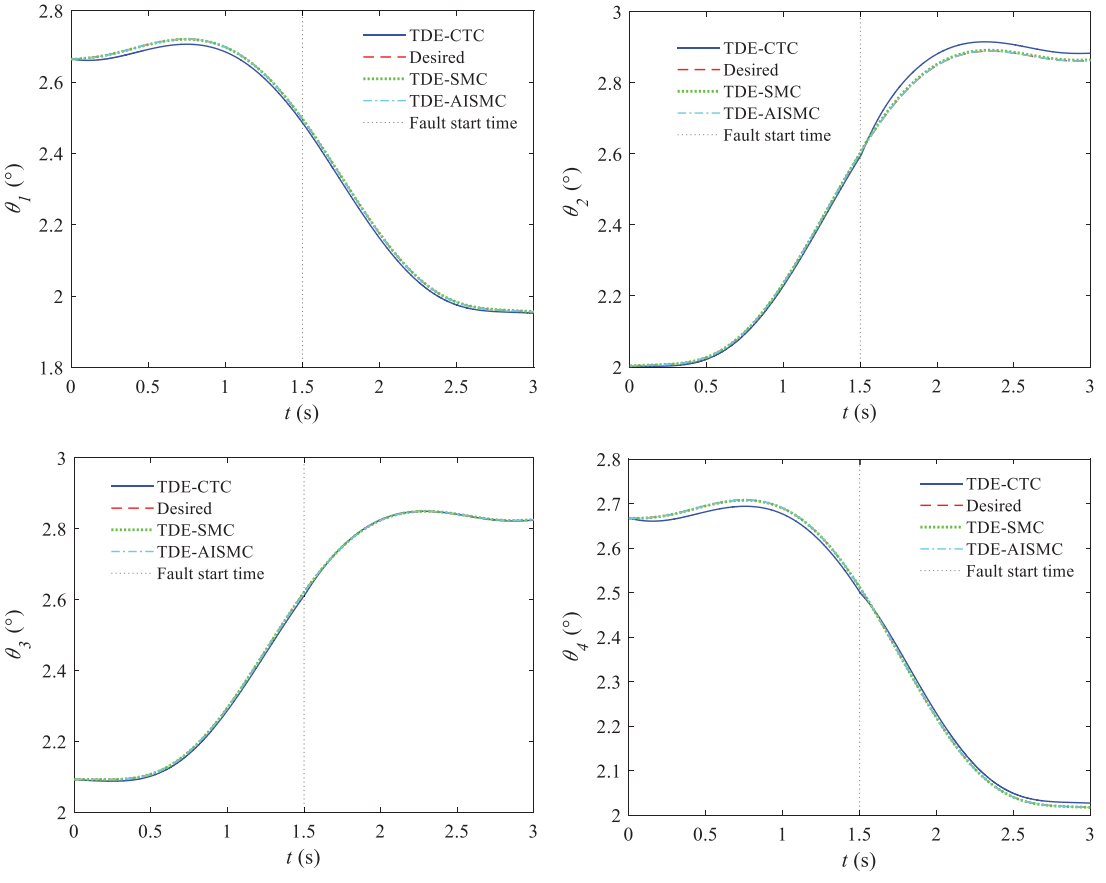

Figure 5. *Active joints trajectories.*

By considering the designed TDE as a robust FD observer, the actuator fault can be detected and isolated in the presence of uncertainties. It is worthy to mention that the FD system not only must be sensitive against any type of fault but also must be robust to cope with uncertainties. To do this, a threshold should be chosen. When $t<L$ then $\mathbf{\Phi}(\mathbf{\Theta}, \dot{\mathbf{\Theta}}, \boldsymbol{\tau}) = \mathbf{0}$, and:

$$\Re_{TDE} = \boldsymbol{\sigma}(\mathbf{\Theta}, \dot{\mathbf{\Theta}}, \boldsymbol{\tau}) \leq \overline{\boldsymbol{\sigma}} = \mathbb{Z}_{threshold} \tag{43}$$

which reveals that the system is in normal condition and the residual $\Re_{TDE}$ is always smaller than $\mathbb{Z}_{threshold}$. Thus, if $\mathbb{Z}_{threshold}$ is chosen as a threshold, the robustness of FD system will be guaranteed. It should be noted that when the residual $\Re_{TDE}$ overshoots its corresponding threshold, the fault can be detected and isolated.

https://doi.org/10.1017/S0263574720001319 Published online by Cambridge University Press

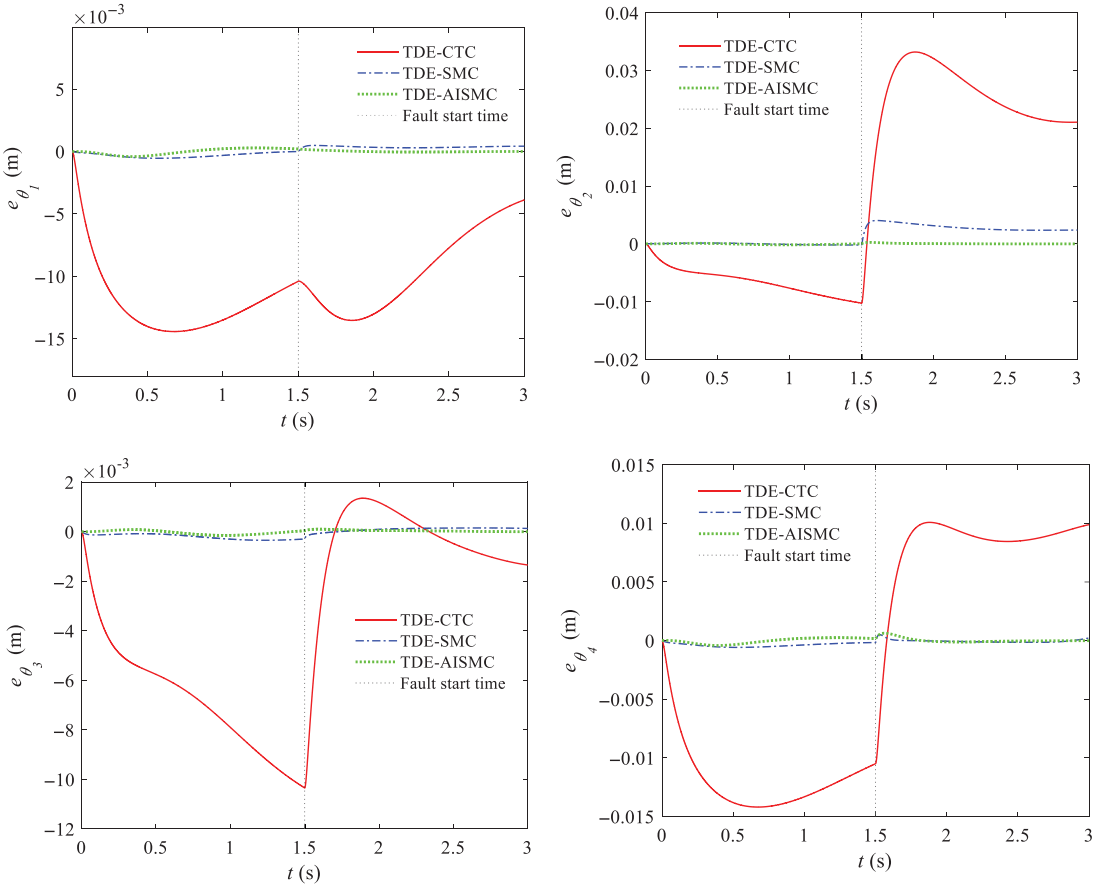

Figure 6. *Active joints tracking errors.*

7. Simulation results

This section is devoted to some simulations demonstrating the effectiveness of the proposed FTC scheme by focusing on trajectory tracking. For this purpose, the tracking performance of the proposed AFTC over a smooth pick-and-place trajectory formed by B-spline is compared with other conventional control schemes, including CTC and SMC. In all simulations, the actuator saturation is also taken into account. Control parameters are listed in Table II.

To verify the capability of the controller for FD, isolation, and compensation, a complex fault, as a combination of actuator bias fault and partial loss of effectiveness, is imposed to the system at $T_f = 1.5$ s, defined by

$$\boldsymbol{\phi} = \begin{bmatrix} 2\theta_2^2 + 5\dot{\theta}_1\theta_3 + 14\sin\dot{\theta}_3 \\ 20\theta_1^2 + 15\,\dot{\theta}_3 + 14\cos\theta_1 \\ 0.3\tau_3 + 6\cos\dot{\theta}_3 \\ 0.3\tau_4 + 6\cos\dot{\theta}_4 \end{bmatrix} \tag{44}$$

The results for actuators trajectories, and their errors are demonstrated in Fig. 5 and Fig. 6. As is obvious from the results, the proposed controller offers the highest level of robustness among the other studied schemes. Moreover, it provides fast convergence to its desired trajectory. CTC, on the other hand, is unable to deal with uncertainties and demonstrates poor performance.

https://doi.org/10.1017/S0263574720001319 Published online by Cambridge University Press

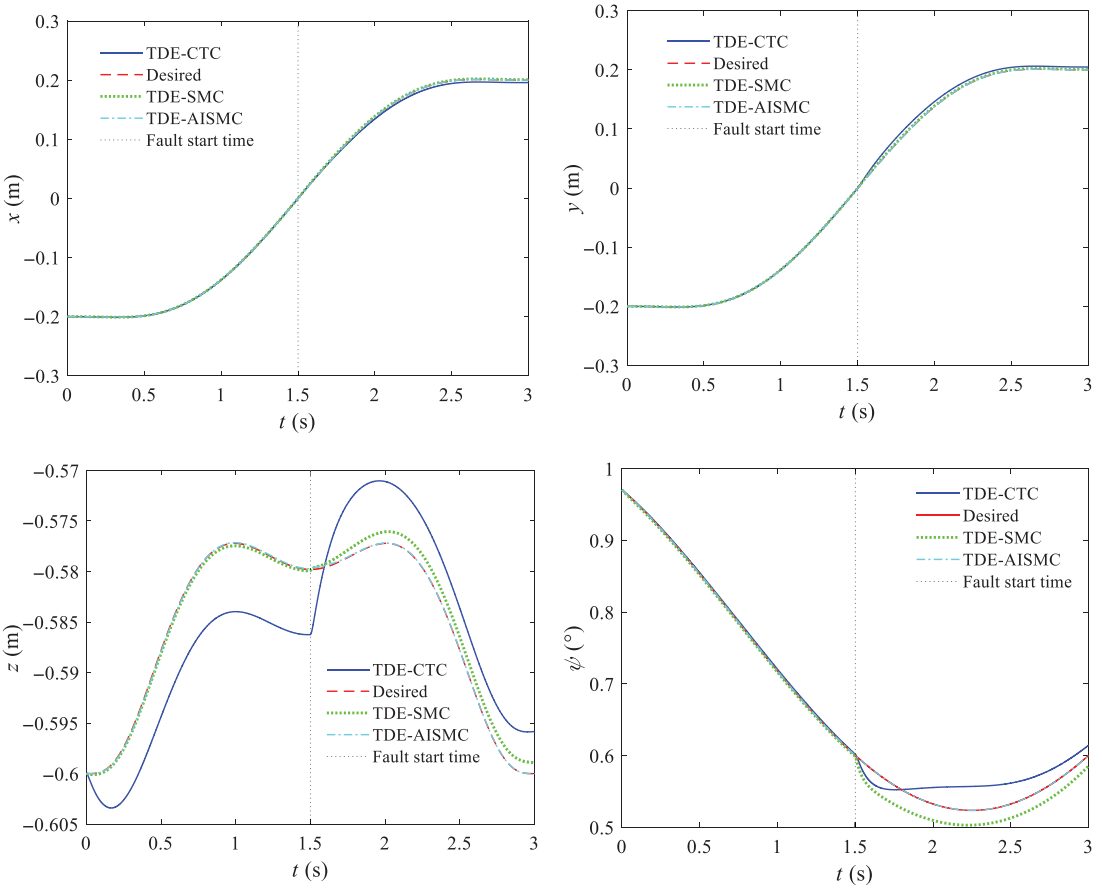

Figure 7. *End-effector trajectory tracking.*

End-effector trajectories tracking and their errors in task space are depicted in Fig. 7 and 8. Similar to joint space, the results reveal that the proposed controller offers good tracking accuracy, while other controllers deviate considerably from the desired trajectory, which is highly noticeable for z and ψ.

Figure 9 shows the desired 3D path and illustrates how it is followed by the robot using different controllers. As the tracking errors implied, the best path following was performed by the ANFITSM controller, while SMC and CTC deviate from the path, with the latter showing poor performance even before fault occurring.

The control commands presented in Fig. 10 reveal a bounded, fluctuation-free pattern of the signal. As the fault occurred at $t = 1.5$ s, the system has experienced an abrupt change, but immediately it has returned to its normal operation.

The FD capability of the AFTC is illustrated in Fig. 11 using extracted residuals. In a normal operation, TDE acts as an uncertainty estimator. Upon fault occurrence at $t = 1.5$ s, the residuals overshoot theirs corresponding thresholds, showing that the FD and isolation are successfully performed.

To better compare the tracking performance of the three control schemes, three error criteria are studied in the presence of faults, namely integral of the time multiplied by the absolute value of the error (ITAE), integral of the time multiplied by the absolute value of the squared of the error (ITASE),

https://doi.org/10.1017/S0263574720001319 Published online by Cambridge University Press

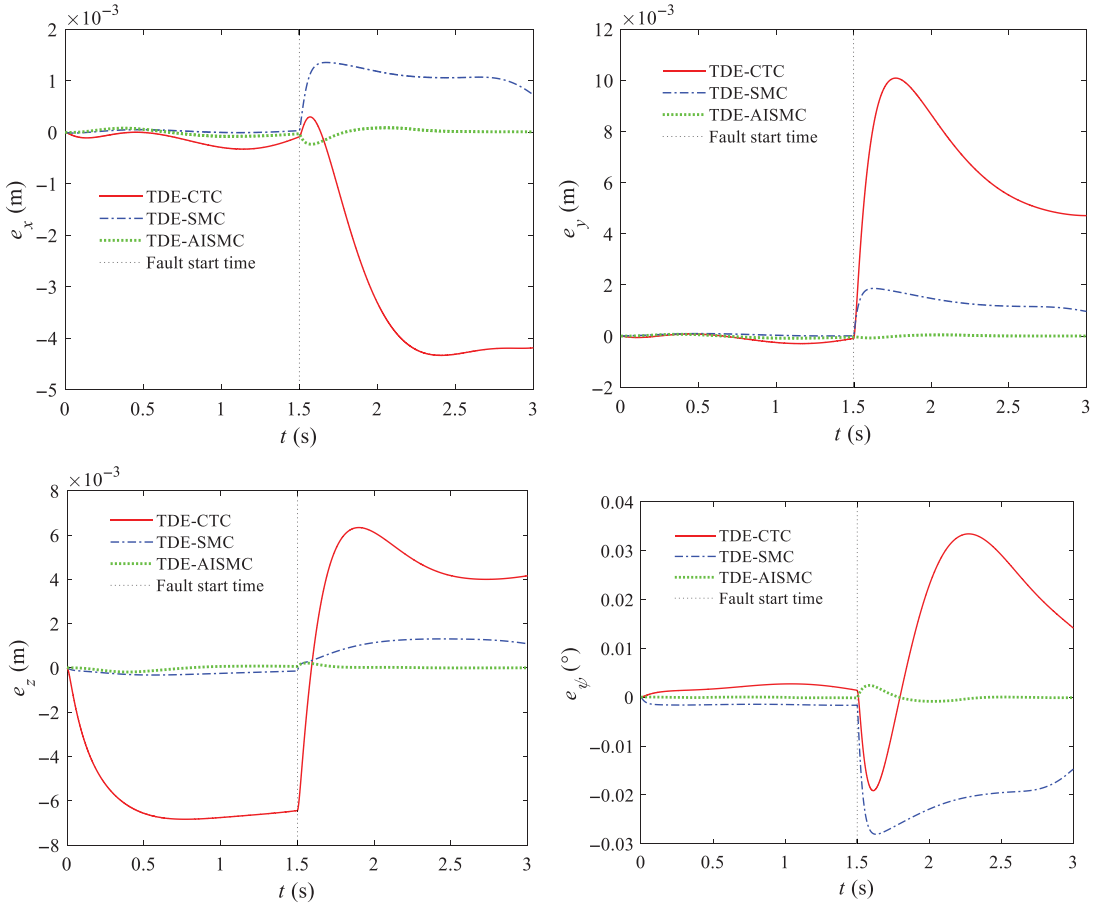

Figure 8. *End-effector tracking errors.*

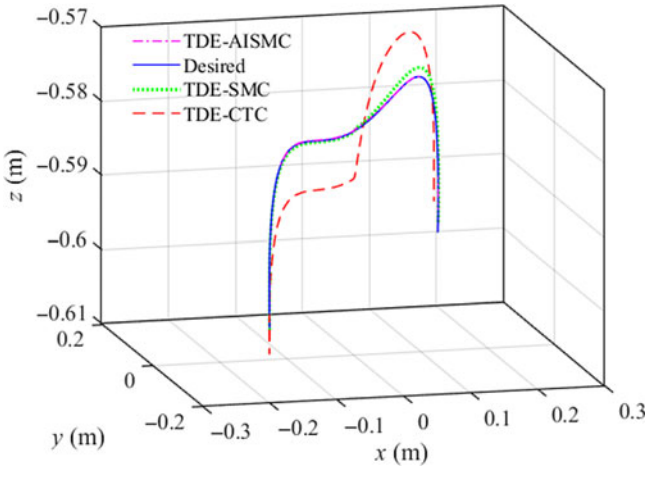

Figure 9. *End-effector path following.*

https://doi.org/10.1017/S0263574720001319 Published online by Cambridge University Press

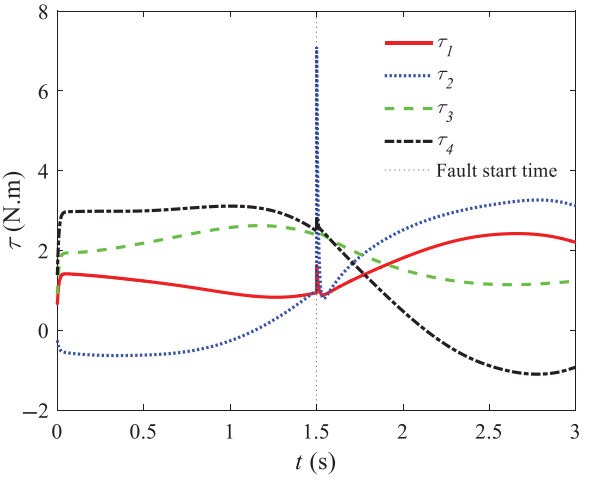

Figure 10. *Actuators' control efforts.*

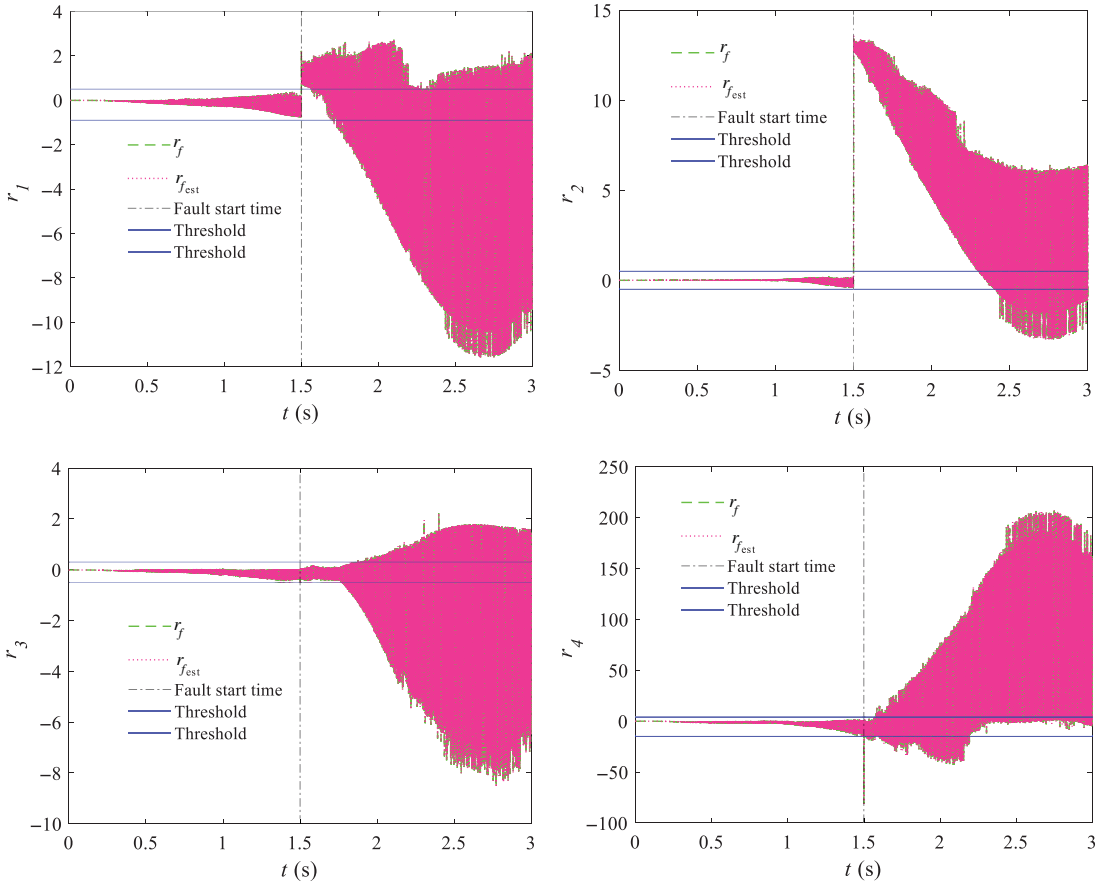

Figure 11. *Residuals.*

https://doi.org/10.1017/S0263574720001319 Published online by Cambridge University Press

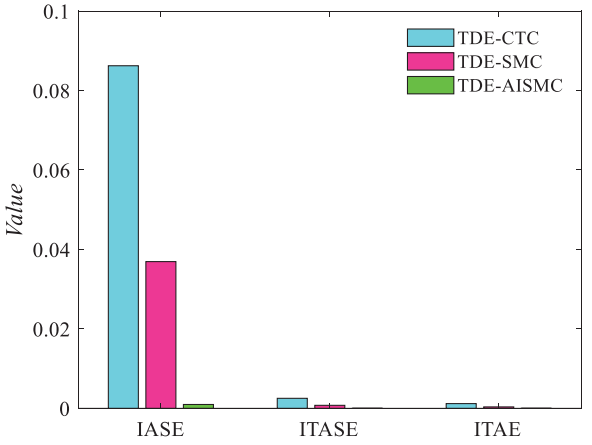

Figure 12. *Error criteria.*

and integral of the absolute value of the squared of the error (IASE). These criteria are defined as follows:

$$ITAE = \int |\boldsymbol{e}(t).t|\, dt$$
$$ITASE = \int t.|\boldsymbol{e}(t)|^2 dt$$
$$IASE = \int |\boldsymbol{e}(t)|^2 dt. \tag{45}$$

The simulation results for these criteria are depicted in Fig. 12. As can be seen, the proposed controller has minimum error for all criteria, and the most significant difference is observed for IASE.

8. Conclusion

In this paper, a new AFTC strategy was designed for a Schoñflies Parallel manipulator by integrating ANFITSM and TDE. For fault diagnosis, TDE was applied which eliminates the requirement for the bound of uncertainty and fault and provides robust performance. The AFTC controller was designed based on ANFITSM, and the stability of the closed-loop system was analyzed using Lyapunov theory. This control scheme ensures high accuracy and robustness, finite-time convergence of the states and eliminates the chattering associated with conventional SMC. The adaptive nature of the controller removes the requirement for the bound of uncertainties. Through some simulations, the proposed controller performance was compared with conventional sliding mode and CTC methods. The obtained results reveal the superiority of the proposed FTC based on TDE and ANFITSM, under uncertainties, external disturbances, and actuator faults.

References

[1] M. Chen and G. Tao, "Adaptive fault-tolerant control of uncertain nonlinear large-scale systems with unknown dead zone," *IEEE Trans. Cybern.* **46**(8), 1851–1862 (2016).
[2] Q. Hu, Y. Shi and X. Shao, "Adaptive fault-tolerant attitude control for satellite reorientation under input saturation, " *Aerospace Sci. Technol.* **78**(1), 171–182 (2018).
[3] Z. Gao, Z. Zhou, M. S. Qian and J. Lin, "Active fault tolerant control scheme for satellite attitude system subject to actuator time-varying faults," **In:** *IET Control Theory Applications* (Institution of Engineering and Technology, 2018) pp. 405–412.
[4] Q. Meng, T. Zhang, X. Gao and J. Song, "Adaptive sliding mode fault-tolerant control of the uncertain stewart platform based on offline multibody dynamics," *IEEE/ASME Trans. Mechatron.* **19**(3), 882–894 (2014).

https://doi.org/10.1017/S0263574720001319 Published online by Cambridge University Press

[5] Q. Meng, T. Zhang, J.-f. He and J.-y. Song, "Adaptive vector sliding mode fault-tolerant control of the uncertain Stewart platform based on position measurements only," *Robotica* **34**(6), 1297–1321 (2016).
[6] Y. Farid, V. J. Majd and A. Ehsani-Seresht, "Fractional-order active fault-tolerant force-position controller design for the legged robots using saturated actuator with unknown bias and gain degradation," Mech. Syst. Signal Process. **104**, 465–486 (2018).
[7] G. C. Karras and G. K. Fourlas, "Model predictive fault tolerant control for omni-directional mobile robots," *J. Intell. Rob. Syst.* **97**(3), 635–655 (2020).
[8] A. Azizi, H. Nourisola and S. Shoja-Majidabad, "Fault tolerant control of wind turbines with an adaptive output feedback sliding mode controller," *Renewable Energy* **135**(1), 55–65 (2019).
[9] J. Lan, R. J. Patton and X. Zhu, "Fault-tolerant wind turbine pitch control using adaptive sliding mode estimation," *Renewable Energy* **116**(1), 219–231 (2018).
[10] S. Cho, Z. Gao and T. Moan, "Model-based fault detection, fault isolation and fault-tolerant control of a blade pitch system in floating wind turbines," *Renewable Energy* **120**(1), 306–321 (2018).
[11] M. Van, M. Mavrovouniotis and S. S. Ge, "An adaptive backstepping nonsingular fast terminal sliding mode control for robust fault tolerant control of robot manipulators," *IEEE Trans. Syst. Man Cybern. Syst.* **49**(7), 1448–1458 (2019).
[12] M. Van and H.-J. Kang, "Robust fault-tolerant control for uncertain robot manipulators based on adaptive quasi-continuous high-order sliding mode and neural network," *Proc. Inst. Mech. Eng. Part C J. Mech. Eng. Sci.* **229**(8), 1425–1446 (2015).
[13] Q. Shen, B. Jiang, P. Shi and C. Lim, "Novel neural networks-based fault tolerant control scheme with fault alarm," *IEEE Trans. Cybern.* **44**(11), 2190–2201 (2014).
[14] Q. Shen, B. Jiang and V. Cocquempot, "Adaptive fuzzy observer-based active fault-tolerant dynamic surface control for a class of nonlinear systems with actuator faults," *IEEE Trans. Fuzzy Syst.* **22**(2), 338–349 (2014).
[15] Z. S. Awan, K. Ali, J. Iqbal and A. Mehmood, "Adaptive backstepping based sensor and actuator fault tolerant control of a manipulator," *J. Electr. Eng. Technol.* **14**(6), 2497–2504 (2019).
[16] P. Shi, M. Liu and L. Zhang, "Fault-tolerant sliding-mode-observer synthesis of Markovian jump systems using quantized measurements," *IEEE Trans. Ind. Electr.* **62**(9), 5910–5918 (2015).
[17] S. Yin, H. Yang and O. Kaynak, "Sliding mode observer-based FTC for Markovian jump systems with actuator and sensor faults," *IEEE Trans. Autom. Control* **62**(7), 3551–3558 (2017).
[18] M. Van, H.-J. Kang and Y.-S. Suh, "A novel neural second-order sliding mode observer for robust fault diagnosis in robot manipulators," *Int. J. Precis. Eng. Manuf.* **14**(3), 397–406 (2013).
[19] M. Van, S. S. Ge and H. Ren, "Finite time fault tolerant control for robot manipulators using Time delay estimation and continuous nonsingular fast terminal sliding mode control," *IEEE Trans. Cybern.* **47**(7), 1681–1693 (2017).
[20] M. Van, H.-J. Kang, Y.-S. Suh and K.-S. Shin, "A robust fault diagnosis and accommodation scheme for robot manipulators," *Int. J. Control Autom. Syst.* **11**(2), 377–388 (2013).
[21] Z. Man, A. P. Paplinski and H. R. Wu, "A robust MIMO terminal sliding mode control scheme for rigid robotic manipulators," *IEEE Trans. Autom. Control* **39**(12), 2464–2469 (1994).
[22] X. Yu and M. Zhihong, "Fast terminal sliding-mode control design for nonlinear dynamical systems," *IEEE Trans. Circuits Syst. I Fundam. Theory Appl.* **49**(2), 261–264 (2002).
[23] Y. Feng, X. Yu and Z. Man, "Non-singular terminal sliding mode control of rigid manipulators," *Automatica* **38**(12), 2159–2167 (2002).
[24] L. Yang and J. Yang, "Nonsingular fast terminal sliding-mode control for nonlinear dynamical systems," *Int. J. Robust Nonlinear Control* **21**(16), 1865–1879 (2011).
[25] M. Mazare, M. Taghizadeh and P. Ghaf-Ghanbari, "Fault-tolerant control based on adaptive super-twisting nonsingular integral-type terminal sliding mode for a delta parallel robot," *J. Braz. Soc. Mech. Sci. Eng.* **42**.8, 1–15 (2020).
[26] M. Van, X. P. Do and M. Mavrovouniotis, "Self-tuning fuzzy PID-nonsingular fast terminal sliding mode control for robust fault tolerant control of robot manipulators," *ISA Trans.* **96**, 60–68 (2020).
[27] Veloce In, "Penta Robotics≫ Products." https://pentarobotics.com/products/ (accessed April 9, 2021).
[28] G. Wu, "Kinematic analysis and optimal design of a wall-mounted four-limb parallel Schönflies-motion robot for pick-and-place operations," *J. Intell. Rob. Syst.* **85**, 663–677 (2017).
[29] Y. Li and Q. Xu, "Kinematics and inverse dynamics analysis for a general 3-PRS spatial parallel mechanism," *Robotica* **23**(2), 219–229 (2005).
[30] Y. Li, T. Huang and D. G. Chetwynd, "An approach for smooth trajectory planning of high-speed pick-and-place parallel robots using quintic B-splines," *Mecha. Mach. Theory* **126**(1), 479–490 (2018).
[31] L. Piegl and W. Tiller, The NURBS Book (Springer-Verlag, Berlin, Heidelberg, 1997).
[32] P.-J. Barre, R. Bearee, P. Borne and E. Dumetz, "Influence of a jerk controlled movement law on the vibratory behaviour of high-dynamics systems," *J. Intell. Rob. Syst.* **42**(3), 275–293 (2005).
[33] M. Jin, S. H. Kang and P. H. Chang, "Robust compliant motion control of robot with nonlinear friction using time-delay estimation," *IEEE Trans. Ind. Electr.* **55**(1), 258–269 (2008).
[34] J. Lee, P. H. Chang and M. Jin, "Adaptive integral sliding mode control with time-delay estimation for robot manipulators," *IEEE Trans. Ind. Electr.* **64**(8), 6796–6804 (2017).
[35] T. C. S. Hsia, "A new technique for robust control of servo systems," *IEEE Trans. Ind. Electr.* **36**(1), 1–7 (1989).

[36] T. C. S. Hsia, T. A. Lasky and Z. Guo, "Robust independent joint controller design for industrial robot manipulators," *IEEE Trans. Ind. Electr.* **38**(1), 21–25 (1991).
[37] J. Lee, P. H. Chang and R. S. Jamisola, "Relative impedance control for dual-arm robots performing asymmetric bimanual tasks," *IEEE Trans. Ind. Electr.* **61**(7), 3786–3796 (2014).
[38] J. Baek, M. Jin and S. Han, "A new adaptive sliding-mode control scheme for application to robot manipulators," *IEEE Trans. Ind. Electr.* **63**(6), 3628–3637 (2016).

Cite this article: P. Ghaf-Ghanbari, M. Mazare and M. Taghizadeh (2021). "Active fault-tolerant control of a Schoñflies parallel manipulator based on time delay estimation", Robotica **39**, 1518–1535. https://doi.org/10.1017/S0263574720001319